A Wearable Inertial Pedestrian Navigation System With Quaternion-Based Extended Kalman Filter for Pedestrian Localization

Yu-Liang Hsu, *Member, IEEE*, Jeen-Shing Wang, *Member, IEEE*, and Che-Wei Chang

***Abstract*— This paper presents a wearable inertial pedestrian navigation system and its associated pedestrian trajectory reconstruction algorithm for reconstructing pedestrian walking trajectories in indoor and outdoor environments. The proposed wearable inertial pedestrian navigation system is constructed by integrating a triaxial accelerometer, a triaxial gyroscope, a triaxial magnetometer, a microcontroller, and a Bluetooth wireless transmission module. Users wear the system on foot while walking in indoor and outdoor environments at normal speed without any external positioning techniques. During walking movement, the measured inertial signals generated from walking movements are transmitted to a computer via the wireless module. Based on the foot-mounted inertial pedestrian navigation system, a pedestrian trajectory reconstruction algorithm composed of the procedures of inertial signal acquisition, signal preprocessing, trajectory reconstruction, and trajectory height estimation has been developed to reconstruct floor walking and stair climbing trajectories. In order to minimize the cumulative error of the inertial signals, we have utilized a sensor fusion technique based on a double-stage quaternion-based extended Kalman filter to fuse acceleration, angular velocity, and magnetic signals. Experimental results have successfully validated the effectiveness of the proposed wearable inertial pedestrian navigation system and its associated pedestrian trajectory reconstruction algorithm.**

***Index Terms*— Inertial positioning system, sensor fusion, pedestrian navigation, quaternion-based extended Kalman filter, pedestrian trajectory reconstruction.**

I. Introduction

RECENTLY, pedestrian navigation systems have gained great attention for their multiple location-based applications. For most existing pedestrian navigation systems, walking velocities and trajectories are obtained through global positioning systems (GPS) measurements. However, GPS is often unavailable in thick forests, urban areas with tall buildings, and indoor environments. Other approaches based on infrastructures such as infrared light, ultrasound, and ultra wide band (UWB) require establishing the initial condition of corresponding sources [1], [2]. One disadvantage of the abovementioned infrastructures is their high cost. In addition, radio frequency identification (RFID) technologies, which are composed of RFID readers and tags, utilize a defined RF to transmit and receive measurements and can also be used in indoor location applications [3]. However, transmission range restrictions and the necessity of numerous readers and tags for accurate positioning limit the effectiveness of RFID for location applications. Wireless local area network (WLAN) is another popular infrastructure for indoor location sensing, but it also requires a large number of access points since location detection accuracy is determined by received signal strength measurements [4].

In recent years, microelectromechanical systems (MEMS)-based inertial and magnetic sensors have become a popular solution for location applications, since they are low cost, small in size, light weight, and have low power consumption [5]–[8]. Huang *et al.* [9] developed a pedestrian tracking system using a small-sized inertial sensor module, which integrates inertial navigation systems (INS) and pedestrian dead-reckoning (PDR) technologies. Likewise, Zhang *et al.* [10] used the features extracted from inertial signals as inputs for a support vector machine (SVM) to classify human step modes and device poses for pedestrian navigation applications, while Meng *et al.* [11] developed a novel self-contained pedestrian tracking method using the zero-velocity updates (ZUPT) and the stride information to improve the tracking accuracy.

To track or reconstruct a spatial walking trajectory, accelerations should be transformed from the body coordinate system to the reference coordinate system [9]. For walking trajectory tracking and reconstruction, the corresponding orientation is required to perform the coordinate transformation. Note that the more accurate the orientation estimation is, the better the trajectory reconstruction result we can obtain. From a review of the literature, we found that some researchers have concentrated on the development of fusion methods with MEMS-based inertial sensors for increasing the accuracy of the orientation estimation [12], [13]. For example, Wang *et al.* [14] presented a quaternion-based Kalman filter (KF) with an accelerometer, a gyroscope, and a magnetometer to estimate the orientation of a quadrotor using an adaptive-step gradient descent algorithm. Sabatelli *et al.* [15] proposed a double-stage quaternion-based KF to estimate orientations by integrating accelerations, angular velocities, and magnetic field measurements. In addition, many researchers have implemented other filters or methods rather than

Manuscript received December 18, 2016; revised February 18, 2017; accepted February 19, 2017. Date of publication March 7, 2017; date of current version April 20, 2017. This work was supported by the Ministry of Science and Technology of China, Taiwan, under MOST 105-3011-E-006-002 and MOST 105-2221-E-035-057. The associate editor coordinating the review of this paper and approving it for publication was Dr. Amitava Chatterjee.

Y.-L. Hsu is with the Department of Automatic Control Engineering, Feng Chia University, Taichung 407, Taiwan.

J. S. Wang and C.-W. Chang are with the Department of Electrical Engineering, National Cheng Kung University, Tainan 701, Taiwan (e-mail: jeenshin@mail.ncku.edu.tw).

Digital Object Identifier 10.1109/JSEN.2017.2679138

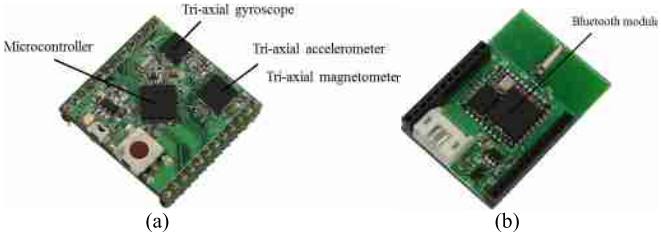

Fig. 1. Wearable inertial pedestrian navigation system. (a) Upper level of the circuit. (b) Lower level of the circuit.

the KF for orientation estimation [16]–[19]. Crassidis and Markley [20] derived an unscented filter for determining the attitude which can be represented by a three-dimensional vector of generalized Rodrigues parameters. Masiero *et al*. [21] utilized a particle filter (PF) to integrate the signals provided by the INS, the standard wireless network, and the geometrical information of the building for estimating indoor human positioning. Fourati [22] developed a novel complementary filter to accurately estimate the foot orientation using the data generated from the accelerometer, angular rate sensors, and magnetometers.

In this study, a wearable inertial pedestrian navigation system and its associated pedestrian trajectory reconstruction algorithm were developed for the purpose of pedestrian navigation in indoor and outdoor environments. Users can wear the system on their foot while walking in indoor and outdoor environments at normal speed without any external positioning techniques. When users wear the wearable system on their foot, walking trajectories can be reconstructed by the pedestrian trajectory reconstruction algorithm which is comprised of the procedures of inertial signal acquisition, signal preprocessing, trajectory reconstruction, and trajectory height estimation. In order to minimize the integral error caused by the intrinsic noise/drift of the inertial sensors, we have utilized a sensor fusion technique based on a double-stage quaternion-based extended Kalman filter (EKF), which was first proposed by Sabatelli *et al*. [15], to fuse the accelerations, angular velocities, and magnetic signals for subsequent correction of the orientation estimation. This method can switch on or off the second stage of the EKF to include or exclude the magnetic signals for separating the effects of a magnetic north on roll and pitch angles' estimation due to the fact that only the estimation of yaw angle is affected. In addition, the velocity error is eliminated through the zero-velocity compensation (ZVC). The main contribution of this algorithm is that it can effectively reduce integral error, and thereby accurately reconstruct and estimate pedestrian walking trajectories in indoor and outdoor environments at normal speed without any external positioning techniques.

The remainder of this paper is organized as follows. In Section II, the hardware architecture of the wearable inertial pedestrian navigation system is introduced. Subsequently, the pedestrian trajectory reconstruction algorithm, composed of inertial signal acquisition, signal preprocessing, trajectory reconstruction, and trajectory height estimation, is presented in Section III. Section IV provides the experimental results of the abovementioned algorithm and validates the effectiveness of the proposed wearable inertial pedestrian navigation system and its associated pedestrian trajectory reconstruction algorithm. Finally, conclusions are presented in Section V.

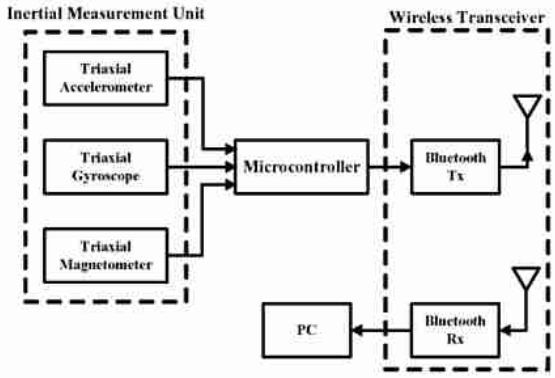

Fig. 2. Schematic diagram of the wearable inertial pedestrian navigation system.

II. Wearable Inertial Pedestrian Navigation System

The inertial pedestrian navigation system developed in this study is a wearable device that can measure and transmit inertial and magnetic signals generated from users' walking motions. This system includes a triaxial accelerometer (LSM303DLH), a triaxial gyroscope (L3G4200D), a triaxial magnetometer (LSM303DLH), an ARM-based 32-bit microcontroller (STM32F217IGH6), and a Bluetooth wireless transmission module. The size of the board, as shown in Fig. 1, is 37.5 mm $\times$ 24 mm $\times$ 10 mm. The accelerometer serves to detect accelerations, velocities, and trajectories of pedestrian walking, while the gyroscope is used to detect the pedestrian walking orientation. In addition, the magnetometer can detect the Earth's magnetic field which is then used to determine the heading during walking. The accelerometer possesses a user selectable full scale of ± 2 g, ± 4 g, and ± 8 g, and its sensitivity is 1 mg/digit. The gyroscope has a full scale of ± 250 °/s, ± 500 °/s, and ± 2000 °/s, and its sensitivity is 8.75×10^{-3} °/s/digit. The magnetometer's full scale is from ± 1.3 gauss to ± 8.1 gauss, and its sensitivity is 1055 digit/gauss. In this paper, the scale ranges of the accelerometer, gyroscope, and magnetometer are set from -4 g to $+4$ g, from -2000 °/s to $+2000$ °/s, and from -1.9 gauss to $+1.9$ gauss, respectively. The microcontroller is responsible for collecting the digital signals generated from the accelerometer, gyroscope, and magnetometer, and for transmitting the signals to a personal computer via the Bluetooth wireless transmission module for further analysis. The digital sampling rate (f_s) of the microcontroller is 75 Hz. The overall power consumption of the hardware device is 30 mA at 3.3 V. The schematic diagram of the wearable inertial pedestrian navigation system is shown in Fig. 2.

III. Pedestrian Trajectory Reconstruction Algorithm

A pedestrian trajectory reconstruction algorithm is developed to reconstruct human walking trajectories by using the

accelerations, angular velocities, and magnetic signals. The pedestrian trajectory reconstruction algorithm is composed of the following procedures: 1) inertial signal acquisition; 2) signal preprocessing; 3) trajectory reconstruction; and 4) trajectory height estimation. At the beginning of the procedures, the signals measured from the accelerometer, gyroscope, and magnetometer are transmitted to a computer via the Bluetooth wireless module. Second, the signal preprocessing of the accelerations, angular velocities, and magnetic signals is performed to eliminate the intrinsic noise and uncertain errors of the sensors, and users' unconscious trembles and walking friction. Third, the trajectory reconstruction procedure utilizes a double-stage quaternion-based extended Kalman filter (EKF) to fuse the filtered accelerations, angular velocities, and magnetic signals for estimating orientations, which can effectively reduce the orientation errors caused by the integral of the drift errors. Once we obtain the quaternion-based orientation via the EKF algorithm, the filtered acceleration can be transformed from the body coordinate system to the reference coordinate system, and the compensation for the gravitational acceleration can be achieved through transformed accelerations. During the static phase detection and zero-velocity compensation (ZVC) steps, the compensated acceleration is used to detect the static phase of each stride by setting an empirical magnitude threshold. Then, the ZVC can be used to reset the velocity to zero in the static phase of each stride in order to reduce the integral of the drift errors [23]. Subsequently, the pedestrian walking trajectory can be reconstructed through the single integral of the compensated velocity. Finally, the trajectory height estimation procedure is used to reconstruct users' trajectories when ascending or descending a flight of stairs. The pedestrian trajectory reconstruction algorithm is shown in Fig. 3.

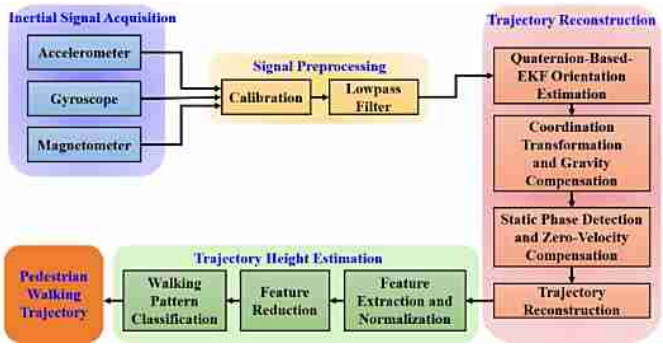

Fig. 3. Pedestrian trajectory reconstruction algorithm.

A. Signal Preprocessing

Due to the contamination of intrinsic noise and uncertain errors of the inertial and magnetic sensors, environmental effects, and users' unconscious trembles and walking friction, signal preprocessing of the measured accelerations, angular velocities, and magnetic signals is required. Since a relatively small drift error or offset on these signals will produce large orientation estimation errors and integral errors, obtaining signals that contain no undesired signal components has become an important issue for pedestrian trajectory reconstruction. In this paper, we first calibrate the accelerometer, gyroscope, and magnetometer, and then filter the high frequency noise of the inertial and magnetic signals via a digital lowpass filter.

1) Calibration: In general, the measurements of the accelerometer, gyroscope, and magnetometer are contaminated by the errors of scale factor and bias, which results in large estimation errors during the trajectory reconstruction [24], [25]. Thus, a calibration procedure for the inertial and magnetic sensors is needed to obtain accurate human walking trajectories. The scale factor (SF) denotes the ratio of change in the output of the sensor to change in the input of the sensor, while the bias (B) denotes the average output of the sensor over a specific time. To obtain the abovementioned calibration parameters (SF and B), the accelerometer, gyroscope, and magnetometer must be placed in at least six positions. When the accelerometer is stationary, the measurement of each sensitive axis of the accelerometer contains only the gravitational acceleration. Thus, we can utilize the gravitational acceleration to calibrate the triaxial accelerometer [24]. However, the Earth's rotation rate cannot be measured by the MEMS-based gyroscope when the gyroscope is stationary. Thus we utilize a rotation stage which can provide a stable rotation rate as a substitute for the Earth's rotation rate as a reference signal for calibrating the triaxial gyroscope. In terms of the magnetometer, the Earth's magnetic field can be used to calibrate the triaxial magnetometer, whose intensity is about 0.3 to 0.4 gauss in Taiwan. However, the magnetic field intensity signal may be contaminated by ferrous materials in the indoor environment. Thus, the Earth's magnetic field intensity is needed to normalize to 1 gauss for reducing the influence of the ferrous materials [26]. We rotate the magnetometer uniformly in a 3-dimensional space to measure the Earth's magnetic field for estimating the calibration parameters [27]. Once the calibration parameters of the accelerometer, gyroscope, and magnetometer are obtained, the accelerations, angular velocities, and magnetic signals can be calibrated as follows:

$$\mathbf{N}_c = \mathbf{C} \cdot \mathbf{N} = \begin{bmatrix} SF_x & 0 & 0 & B_x \\ 0 & SF_y & 0 & B_y \\ 0 & 0 & SF_z & B_z \end{bmatrix} \mathbf{N}, \tag{1}$$

where $\mathbf{C}$ represents the calibration matrix of the accelerometer ($\mathbf{C}_a$), gyroscope ($\mathbf{C}_g$), and magnetometer ($\mathbf{C}_m$), SF_x, SF_y, and SF_z are the scale factors, and B_x, B_y, and B_z are the biases of each axis of the accelerometer, gyroscope, and magnetometer, $\mathbf{N}$ represents the uncalibrated accelerations ($\mathbf{A} = [\,A_x,\ A_y,\ A_z,\ 1\,]^T$ with the unit of g), angular velocities ($\boldsymbol{\omega} = [\,\omega_x,\ \omega_y,\ \omega_z,\ 1\,]^T$ with the unit of rad/sec), or magnetic signals ($\mathbf{M} = \left[\,M_x,\ M_y,\ M_z,\ 1\,\right]^T$ with the unit of gauss), and $\mathbf{N}_c$ represents the calibrated accelerations ($\mathbf{A}_c = [\,A_{cx},\ A_{cy},\ A_{cz}\,]^T$ with the unit of g), angular velocities ($\boldsymbol{\omega}_c = [\,\omega_{cx},\ \omega_{cy},\ \omega_{cz}\,]^T$ with the unit of rad/sec), or magnetic signals ($\mathbf{M}_c = \left[\,M_{cx},\ M_{cy},\ M_{cz}\,\right]^T$ with the unit of gauss).

2) Lowpass Filter: After the calibration process is completed, a moving average filter is used to reduce the high-frequency noise of the accelerations, angular velocities and magnetic signals generated from users' unconscious trembles and walking friction. The moving average filter is

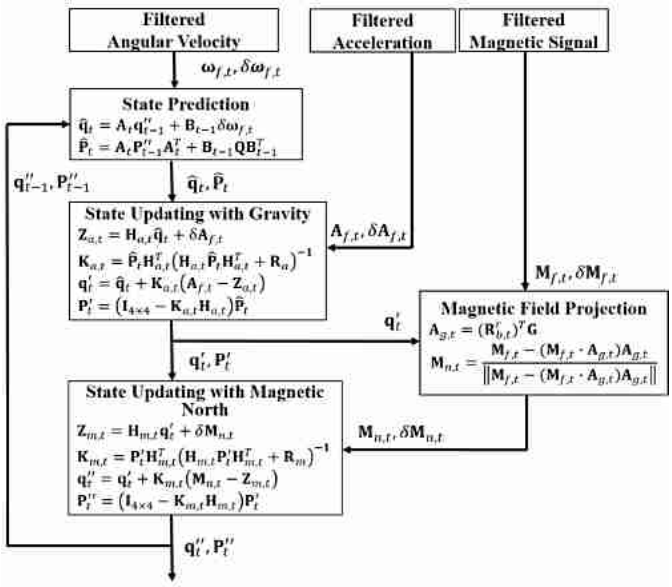

Fig. 4. The double-stage quaternion-based extended Kalman filter algorithm.

expressed as

$$y[n] = \frac{1}{N}\sum_{i=1}^{N} x[n-i], \tag{2}$$

where $x[n]$ represents calibrated accelerations, angular velocities, or magnetic signals, $y[n]$ represents the filtered accelerations, angular velocities, and magnetic signals, denoted as $\mathbf{A}_f = [A_{fx}, A_{fy}, A_{fz}]^T$, $\boldsymbol{\omega}_f = [\omega_{fx}, \omega_{fy}, \omega_{fz}]^T$, or $\mathbf{M}_f = \left[M_{fx}, M_{fy}, M_{fz}\right]^T$, and N is the number of points in the average filter. In this paper, according to our empirical tests, we set $N = 5$.

B. Trajectory Reconstruction

The trajectory reconstruction procedure involves the following steps: 1) quaternion-based extended Kalman filter orientation estimation, 2) coordinate transformation and gravity compensation, 3) static phase detection and zero-velocity compensation, and 4) trajectory reconstruction. We describe each step in detail as follows.

1) Quaternion-Based Extended Kalman Filter Orientation Estimation: Once we obtain the filtered accelerations, angular velocities, and magnetic signals measured from the foot-mounted wearable inertial pedestrian navigation system during walking, a double-stage quaternion-based EKF is utilized to estimate the orientation angles of user's movement by fusing these signals in this paper [15]. The double-stage EKF weights the accelerations, angular velocities, and magnetic signals appropriately with the signal characteristic based on the model which best makes use of the measurement signals from each of the sensors. To reconstruct a walking trajectory, the filtered accelerations must be transferred from the body coordinate system to the reference coordinate system. For the pedestrian walking trajectory, the corresponding orientation is required to perform the coordinate transformation. Note that the more accurate the orientation estimation is, the better the resulting trajectory reconstruction that is obtained. The double-stage quaternion-based EKF algorithm used in this paper is shown in Fig. 4. The quaternion representation is employed to express the orientation angles of the navigation system in order to avoid the numerical singularity of the Euler angles [28]. In general, the quaternion must obey a unit norm constraint, that is, $|\mathbf{q}| = \sqrt{q_0^2 + q_1^2 + q_2^2 + q_3^2}$. The detailed procedures can be found in [15]. The double-stage quaternion-based EKF composed of state prediction, state updating with gravity, and state updating with magnetic north is summarized as follows. More detailed information for the double-stage quaternion-based EKF can be found in [15].

a) State prediction:

1) Obtain the filtered angular velocity $\boldsymbol{\omega}_{f,t} = [\omega_{fx}, \omega_{fy}, \omega_{fz}]_t^T$ and its white noise $\delta\boldsymbol{\omega}_{f,t} = [\delta\omega_{fx}, \delta\omega_{fy}, \delta\omega_{fz}]_t^T$.
2) Calculate the state transition matrix ($\mathbf{A}_t$) and coefficient matrix ($\mathbf{B}_{t-1}$).

$$\mathbf{A}_t = \mathbf{I}_{4\times4} + \frac{1}{2}\boldsymbol{\Omega}(\boldsymbol{\omega}_{f,t})T_s, \tag{3}$$

$$\mathbf{B}_{t-1} = \frac{1}{2}T_s\begin{bmatrix} -q_1'' & -q_2'' & -q_3'' \\ q_0'' & q_3'' & q_2'' \\ q_3'' & q_0'' & -q_1'' \\ -q_2'' & q_1'' & q_0'' \end{bmatrix}_{t-1}, \tag{4}$$

where

$$\boldsymbol{\Omega}(\boldsymbol{\omega}_{f,t}) = \begin{bmatrix} 0 & -\omega_{fx} & -\omega_{fy} & -\omega_{fz} \\ \omega_{fx} & 0 & \omega_{fz} & -\omega_{fy} \\ \omega_{fy} & -\omega_{fz} & 0 & \omega_{fx} \\ \omega_{fz} & \omega_{fy} & -\omega_{fx} & 0 \end{bmatrix}_t,$$

$$\mathbf{q}''_{t-1} = [q_0'', \quad q_1'', \quad q_2'', \quad q_3'']_{t-1}^T$$

represents the quaternion-based orientation at the preceding time step, and T_s is the sampling time ($T_s = 1/f_s$).

3) Obtain the state equation to predict the quaternion-based orientation ($\hat{\mathbf{q}}_t = [\hat{q}_0, \hat{q}_1, \hat{q}_2, \hat{q}_3]_t^T$) at the present time step.

$$\hat{\mathbf{q}}_t = \mathbf{A}_t\mathbf{q}''_{t-1} + \mathbf{B}_{t-1}\delta\boldsymbol{\omega}_{f,t}. \tag{5}$$

4) Estimate the state error covariance matrix ($\hat{\mathbf{P}}_t$) at the present time step.

$$\hat{\mathbf{P}}_t = \mathbf{A}_t\mathbf{P}''_{t-1}\mathbf{A}_t^T + \mathbf{B}_{t-1}\mathbf{Q}\mathbf{B}_{t-1}^T, \tag{6}$$

where $\mathbf{P}''_{t-1}$ is the state error covariance matrix at the preceding time step, and $\mathbf{Q} = E[\delta\boldsymbol{\omega}_f\delta\boldsymbol{\omega}_f^T]$ is the white noise covariance matrix of the filtered angular velocity.

b) State updating with gravity:

1) Calculate the gravity observation matrix ($\mathbf{H}_{a,t}$).

$$\mathbf{H}_{a,t} = 2\begin{bmatrix} -\hat{q}_2 & \hat{q}_3 & -\hat{q}_0 & \hat{q}_1 \\ \hat{q}_1 & \hat{q}_0 & \hat{q}_3 & \hat{q}_2 \\ \hat{q}_0 & -\hat{q}_1 & -\hat{q}_2 & \hat{q}_3 \end{bmatrix}_t. \tag{7}$$

2) Obtain the filtered acceleration $\mathbf{A}_{f,t} = [A_{fx}, A_{fy}, A_{fz}]_t^T$ and its white noise $\delta\mathbf{A}_{f,t} = [\delta A_{fx}, \delta A_{fy}, \delta A_{fz}]_t^T$.

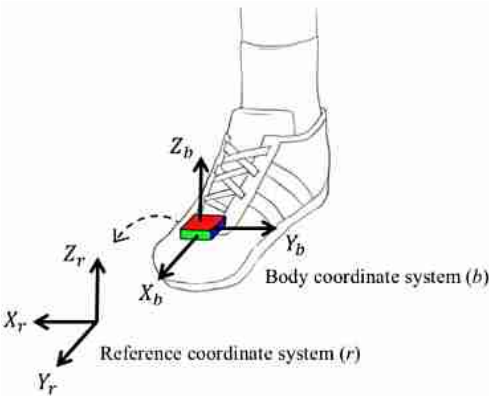

Fig. 5. Coordinate transformation.

3) Calculate the Kalman gain of the gravity updating ($\mathbf{K}_{a,t}$).

$$\mathbf{K}_{a,t} = \hat{\mathbf{P}}_t \mathbf{H}_{a,t}^T (\mathbf{H}_{a,t} \hat{\mathbf{P}}_t \mathbf{H}_{a,t}^T + \mathbf{R}_a)^{-1}, \tag{8}$$

where $\mathbf{R}_a = E[\delta \mathbf{A}_f \delta \mathbf{A}_f^T]$ is the white noise covariance matrix of the filtered acceleration.

4) Obtain the gravity observation equation to calculate the gravity observation ($\mathbf{Z}_{a,t} = [\, Z_{ax},\, Z_{ay},\, Z_{az}\,]_t^T$).

$$\mathbf{Z}_{a,t} = \mathbf{H}_{a,t} \hat{\mathbf{q}}_t + \delta \mathbf{A}_{f,t}. \tag{9}$$

5) Use the Kalman gain of the gravity updating ($\mathbf{K}_{a,t}$) to adjust the correct factor $\mathbf{q}_\epsilon = [\, q_0,\, q_1,\, q_2,\, q_3\,]_\epsilon^T$.

$$\mathbf{q}_\epsilon = \mathbf{K}_{a,t} (\mathbf{A}_{f,t} - \mathbf{Z}_{a,t}), \tag{10}$$

where $q_{\epsilon 3}$ is equal to zero [15].

6) Update the predicted state ($\hat{\mathbf{q}}_t$) to obtain the quaternion-based orientation of the gravity updating ($\mathbf{q}_t' = [\, q_0',\, q_1',\, q_2',\, q_3'\,]_t^T$).

$$\mathbf{q}_t' = \hat{\mathbf{q}}_t + \mathbf{q}_\epsilon. \tag{11}$$

7) Update the state error covariance matrix ($\hat{\mathbf{P}}_t$) to obtain the state error covariance matrix of the gravity updating ($\mathbf{P}_t'$).

$$\mathbf{P}_t' = (\mathbf{I}_{4\times 4} - \mathbf{K}_{a,t} \mathbf{H}_{a,t}) \hat{\mathbf{P}}_t. \tag{12}$$

c) State updating with magnetic north:

1) Calculate the magnetic north observation matrix ($\mathbf{H}_{m,t}$).

$$\mathbf{H}_{m,t} = 2 \begin{bmatrix} q_3' & q_2' & q_1' & q_0' \\ q_0' & -q_1' & q_2' & -q_3' \\ -q_1' & -q_0' & q_3' & q_2' \end{bmatrix}_t. \tag{13}$$

2) Obtain the filtered magnetic signal $\mathbf{M}_{f,t} = [\, M_{fx},\, M_{fy},\, M_{fz}\,]_t^T$, and calculate the magnetic north vector $\mathbf{M}_{n,t} = [\, M_{nx},\, M_{ny},\, M_{nz}\,]_t^T$ and its white noise $\delta \mathbf{M}_{n,t} = [\, \delta M_{nx},\, \delta M_{ny},\, \delta M_{nz}\,]_t^T$. First, we use the quaternion-based orientation of the gravity update ($\mathbf{q}_t'$) to construct a transformation matrix from the body coordinate system to the reference coordinate system ($\mathbf{R}_{b,t}^r$). Then, we take the inverse transformation of the gravitational acceleration ($\mathbf{G}$) from the reference coordinate system to the body coordinate system to estimate the gravitational acceleration in the body coordinate system ($\mathbf{A}_{g,t}$) by the following equation:

$$\mathbf{A}_{g,t} = (\mathbf{R}_{b,t}^r)^T \mathbf{G}, \tag{14}$$

where $\mathbf{G} = [\, 0,\, 0,\, 1\,]^T$ with the unit of g is the gravitational acceleration in the East, North, Up (ENU) reference coordinate system. Finally, we project the filtered magnetic signal ($\mathbf{M}_{f,t}$) on the gravitational acceleration in the body coordinate system ($\mathbf{A}_{g,t}$), and obtain the magnetic north vector ($\mathbf{M}_{n,t}$) by the following equation:

$$\mathbf{M}_{n,t} = \frac{\mathbf{M}_{f,t} - (\mathbf{M}_{f,t} \cdot \mathbf{A}_{g,t}) \mathbf{A}_{g,t}}{\left\| \mathbf{M}_{f,t} - (\mathbf{M}_{f,t} \cdot \mathbf{A}_{g,t}) \mathbf{A}_{g,t} \right\|}. \tag{15}$$

3) Calculate the Kalman gain of the magnetic north updating ($\mathbf{K}_{m,t}$).

$$\mathbf{K}_{m,t} = \mathbf{P}_t' \mathbf{H}_{m,t}^T (\mathbf{H}_{m,t} \mathbf{P}_t' \mathbf{H}_{m,t}^T + \mathbf{R}_m)^{-1}, \tag{16}$$

where $\mathbf{R}_m = E[\delta \mathbf{M}_n \delta \mathbf{M}_n^T]$ is the white noise covariance matrix of the magnetic north vector.

4) Obtain the magnetic north observation equation to calculate the magnetic north observation ($\mathbf{Z}_{m,t} = [\, Z_{mx},\, Z_{my},\, Z_{mz}\,]_t^T$)

$$\mathbf{Z}_{m,t} = \mathbf{H}_{m,t} \mathbf{q}_t' + \delta \mathbf{M}_{n,t}. \tag{17}$$

5) Use the Kalman gain of the magnetic north updating ($\mathbf{K}_{m,t}$) to adjust the correct factor $\mathbf{q}_\epsilon' = [\, q_0',\, q_1',\, q_2',\, q_3'\,]_\epsilon^T$.

$$\mathbf{q}_\epsilon' = \mathbf{K}_{m,t} (\mathbf{M}_{n,t} - \mathbf{Z}_{m,t}), \tag{18}$$

where $q_{\epsilon 1}'$ and $q_{\epsilon 2}'$ are equal to zero [15].

6) Adjust the state of the gravity updating ($\mathbf{q}_t'$) to obtain the quaternion-based orientation of the magnetic north updating ($\mathbf{q}_t'' = [\, q_0'',\, q_1'',\, q_2'',\, q_3''\,]_t^T$).

$$\mathbf{q}_t'' = \mathbf{q}_t' + \mathbf{q}_\epsilon'. \tag{19}$$

7) Adjust the state error covariance matrix of the gravity updating ($\mathbf{P}_t'$) to obtain the state error covariance matrix of the magnetic north updating ($\mathbf{P}_t''$).

$$\mathbf{P}_t'' = (\mathbf{I}_{4\times 4} - \mathbf{K}_{m,t} \mathbf{H}_{m,t}) \mathbf{P}_t'. \tag{20}$$

2) Coordinate Transformation and Gravity Compensation: Due to the fact that the accelerations measured by the accelerometer during walking always contains the gravitational acceleration which must be subtracted from the measured acceleration to obtain the acceleration generated by motion alone. Since the orientation of the foot-mounted wearable inertial pedestrian navigation system changes dynamically during walking to perform the aforementioned subtraction, all the filtered accelerations have to transfer from the body coordinate system to the reference coordinate system. The reference coordinate system used in this paper is the East, North, Up (ENU) coordinate system. The coordinate transformation of the wearable inertial pedestrian navigation system is shown in Fig. 5. To transform the filtered acceleration from the body coordinate system to the reference coordinate system, we need to derive a transformation matrix ($\mathbf{R}_b^r$) based on

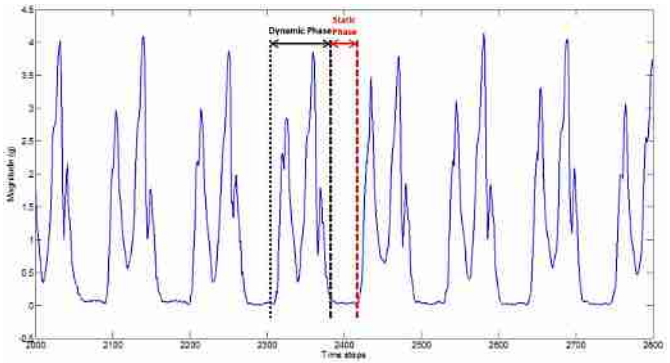

Fig. 6. SVM of the compensated acceleration.

the quaternion that represents the wearable inertial pedestrian navigation system's orientation in the reference coordinate system, which is obtained by the double-stage quaternion-based EKF.

$$\mathbf{R}_b^r = \begin{bmatrix} q_0^2+q_1^2-q_2^2-q_3^2 & 2(q_1q_2-q_0q_3) & 2(q_1q_3+q_0q_2) \\ 2(q_1q_2+q_0q_3) & q_0^2-q_1^2+q_2^2-q_3^2 & 2(q_2q_3-q_0q_1) \\ 2(q_1q_3-q_0q_2) & 2(q_2q_3+q_0q_1) & q_0^2-q_1^2-q_2^2+q_3^2 \end{bmatrix}. \tag{21}$$

With the transformation matrix ($\mathbf{R}_b^r$), we can transfer the filtered acceleration from the body coordinate system to the reference coordinate system as follows:

$$\mathbf{A}_r = \mathbf{R}_b^r \mathbf{A}_f, \tag{22}$$

where $\mathbf{A}_f = [\, A_{fx},\ A_{fy},\ A_{fz}\,]^T$ is the filtered acceleration in the body coordinate system and $\mathbf{A}_r = [\, A_{rx},\ A_{ry},\ A_{rz}\,]^T$ is the transformed acceleration in the reference coordinate system. Subsequently, the compensated acceleration in the reference coordinate system generated from walking is then expressed as follows:

$$\mathbf{A}_{rc} = \mathbf{A}_r - \mathbf{G}, \tag{23}$$

where $\mathbf{A}_{rc} = [\, A_{rcx},\ A_{rcy},\ A_{rcz}\,]^T$ is the compensated acceleration in the reference coordinate system and $\mathbf{G} = [\, 0,\ 0,\ 1\,]^T$ with the unit of g is the gravitational acceleration in the ENU reference coordinate system, which is the mean of the transformed acceleration for each axis in the ENU reference coordinate system when the device is stationary.

3) Static Phase Detection and Zero-Velocity Compensation: Walking is a periodic motion for which each stride can be further divided into two periods: a static phase and a dynamic phase [29]. Specifically, the static phase is the entire period during which the foot is on the ground and the walking velocity is equal to zero in ideal circumstances. Based on this fact, we can reset the velocity in the static phase to reduce the cumulative integral error of the drift error of the compensated acceleration during each stride. In this paper, we develop a magnitude threshold method for detecting the static phase based on a magnitude threshold of the signal vector magnitude (SVM) of the compensated acceleration. Then, the zero-velocity compensation (ZVC) is used to adjust

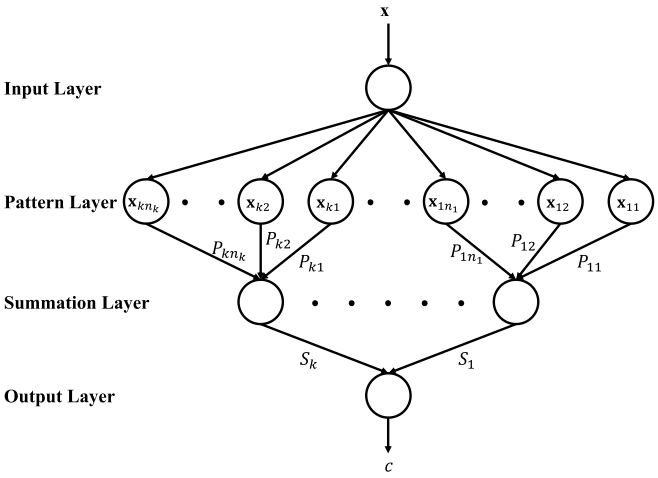

Fig. 7. Structure of probabilistic neural network classifier.

the velocity error to compensate the integral error of the drift error of the compensated acceleration [23]. The SVM of the compensated acceleration is defined as follows:

$$A_{svm} = \sqrt{A_{rcx}^2 + A_{rcy}^2 + A_{rcz}^2}. \tag{24}$$

Fig. 6 shows the SVM of the compensated acceleration in the reference coordinate system. Obviously, the SVM of the compensated acceleration within the static phase approximates to zero, while that within the dynamic phase changes dynamically. Therefore, an empirical magnitude threshold for the SVM of the compensated acceleration is set at 0.05g to distinguish the static phase and dynamic phase. In addition, the start and end points of each dynamic phase must be determined based on the following assumption: The SVM of the compensated acceleration should be higher or lower than the magnitude threshold and maintain at least 10 time steps continuously to avoid the influence of users' unconscious foot trembles. Once the SVMs of the compensated accelerations within the 10 time steps are all higher than the threshold, the first sample point of the 10 time steps can be designated as the start point of a dynamic phase within a stride. Similarly, the end point of a dynamic phase within a stride can be determined when the SVMs of the compensated accelerations within the 10 time steps are all lower than the threshold. Once we can obtain the dynamic phase, the static phase within the stride can also be determined. Subsequently, the velocity of walking motions can be obtained through the single integral of the compensated acceleration as (25). Particularly, the velocity must be zero in the static phase and the ZVC can be used to compensate the error of the velocity in the dynamic phase, which is obtained by integrating the drift error of the compensated acceleration as follows:

$$\mathbf{V}_t = \mathbf{V}_{t-1} + \frac{1}{2} T_s (\mathbf{A}_{rc,t} + \mathbf{A}_{rc,t-1}), \tag{25}$$

$$\mathbf{V}_{c,t} = \mathbf{V}_t - \frac{\mathbf{V}_{t_{end}}}{t_{end} - t_{start}} (t - t_{start}), \tag{26}$$

where t and $t-1$ represent the present and preceding time steps, T_s is the sampling time, $\mathbf{A}_{rc} = [\, A_{rcx},\ A_{rcy},\ A_{rcz}\,]^T$

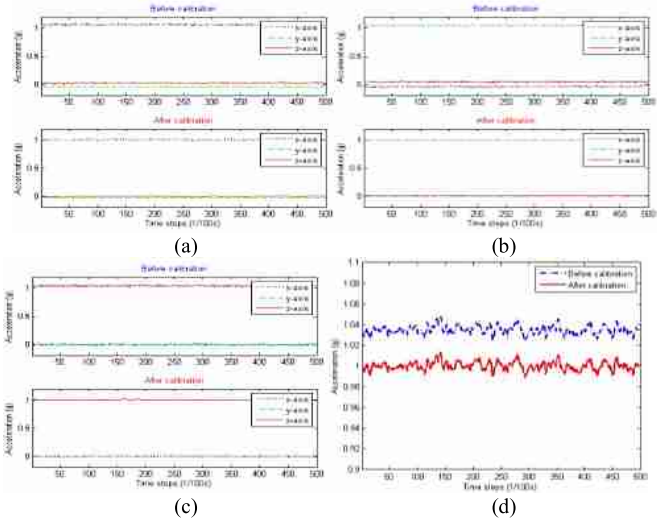

Fig. 8. Experimental results of the accelerometer calibration process. The signals of each axis of the triaxial accelerometer aligned with the Earth's gravity. (a) x-axis accelerations. (b) y-axis accelerations. (c) z-axis accelerations. (d) The SVM of the accelerations.

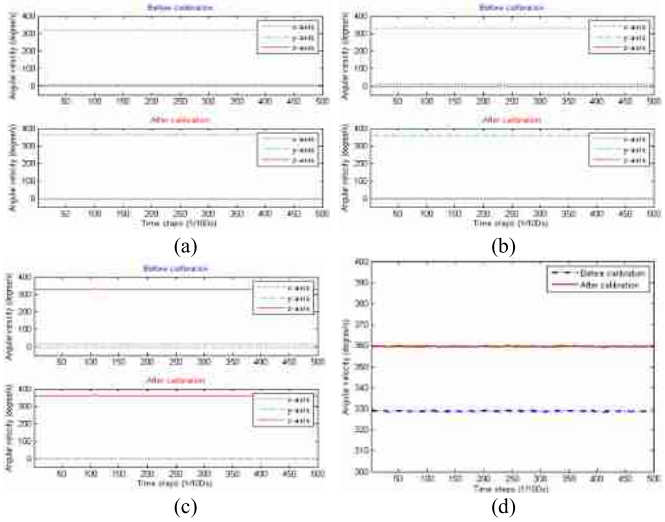

Fig. 9. Experimental results of the gyroscope calibration process. (a) The signals of the gyroscope rotated around x-axis at a rate of 360 °/s. (b) The signals of the gyroscope rotated around y-axis at a rate of 360 °/s. (c) The signals of the gyroscope rotated around z-axis at a rate of 360 °/s. (d) The SVM of the angular velocities when the gyroscope was placed randomly and rotated at a rate of 360 °/s.

is the compensated acceleration, $\mathbf{V}_t = [\,V_x,\, V_y,\, V_z\,]_t^T$ is the velocity, t_{start} and t_{end} are the start and end points of the dynamic phase, $\mathbf{V}_{t_{end}} = [\,V_x,\, V_y,\, V_z\,]_{t_{end}}^T$ represents the velocity at the end point of the dynamic phase, and $\mathbf{V}_{c,t} = [\,V_{cx},\, V_{cy},\, V_{cz}\,]_t^T$ represents the compensated velocity.

4) Trajectory Reconstruction: Once the velocity has been obtained through the single integral of the compensated acceleration and compensated by the ZVC, we can derive the pedestrian position or trajectory through the single integral of the compensated velocity as follows:

$$\mathbf{L}_t = \mathbf{L}_{t-1} + \frac{1}{2} T_s (\mathbf{V}_{c,t} + \mathbf{V}_{c,t-1}), \tag{27}$$

where $\mathbf{V}_{c,t} = [\,V_{cx},\, V_{cy},\, V_{cz}\,]_t^T$ represents the compensated velocity, T_s is the sampling time, $\mathbf{L}_{t-1} = [\,L_x,\, L_y,\, L_z\,]_{t-1}^T$ represents the position or trajectory at preceding time step, and $\mathbf{L}_t = [\,L_x,\, L_y,\, L_z\,]_t^T$ represents the position or trajectory at present time step.

C. Trajectory Height Estimation

To reconstruct the pedestrian trajectory during stair climbing inside the building, the vertical height of the walking trajectory can be derived through the double integral of the z-axis compensated acceleration theoretically. However, the z-axis compensated acceleration measured by the triaxial accelerometer contains the acceleration generated from the reaction of the walking motions when the pedestrian walks upstairs and downstairs, which causes enormous error for height estimation. In this paper, we developed a trajectory height estimation algorithm to classify walking patterns using the compensated walking velocity in each dynamic phase within each stride as level walking, walking upstairs, or walking downstairs. Once the number of the strides of the level walking, walking upstairs, and walking downstairs are obtained by the developed trajectory height estimation algorithm, the pedestrian trajectory of stair climbing inside the building can be determined directly [30]. The trajectory height estimation procedure is composed of the following steps: 1) feature extraction and normalization, 2) feature reduction, and 3) probabilistic neural network (PNN) classifier. We describe each step in detail as follows.

1) Feature Extraction and Normalization: Once the compensated velocity of each dynamic phase of each stride is obtained, the gait features of each stride can be extracted from the x-, y-, and z-axis compensated velocity, respectively. The gait features including 1) mean (*MEAN*), 2) standard deviation (*SD*), 3) variance (*VAR*), 4) mean absolute deviation (*MAD*), 5) root mean square (*RMS*), 6) interquartile range (*IQR*), and 7) correlation coefficient (*CC*), are used for classifying the walking patterns.

- *Mean (MEAN)*: The mean value of the compensated velocity in each dynamic phase of each stride is calculated as follows:

$$MEAN = \bar{V}_c = \frac{1}{N} \sum_{i=1}^{N} V_{ci}, \tag{28}$$

- *Standard deviation (SD):* The standard deviation value is the square root of the variance value.

$$SD = \sqrt{\frac{\sum_{i=1}^{N} (V_{ci} - \bar{V}_c)^2}{N-1}}, \tag{29}$$

- *Variance (VAR):*

$$VAR = \frac{\sum_{i=1}^{N} (V_{ci} - \bar{V}_c)^2}{N-1}, \tag{30}$$

- *Mean absolute deviation (MAD):*

$$MAD = \frac{\sum_{i=1}^{N} \left| V_{ci} - \bar{V}_c \right|}{N}, \tag{31}$$

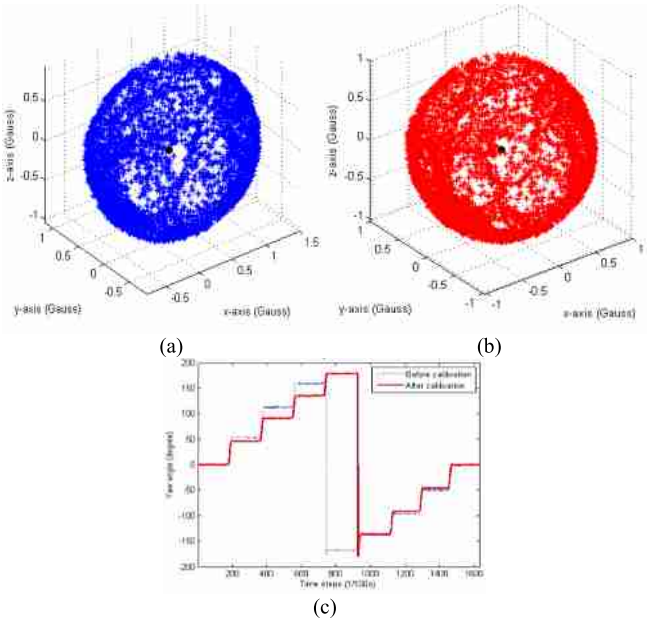

Fig. 10. Experimental results of the magnetometer calibration process. (a) The magnetic signals in a 3D space before the calibration. (b) The magnetic signals in a 3D space after the calibration. (c) Yaw angles estimated by the magnetic signals.

- *Root mean square (RMS):*

$$RMS = \sqrt{\frac{\sum_{i=1}^{N} V_{ci}^2}{N}}, \tag{32}$$

where V_{ci} is the compensated velocity of each axis in each dynamic phase of each stride, $\bar{V}_c$ is the mean value of V_{ci}, and N is the number of measurements in each dynamic phase of each stride in (28)-(32).

- *Interquartile range (IQR):* The interquartile range value is the difference between the 75th percentile value and the 25th percentile value of the compensated velocity of each axis in each dynamic phase of each stride.
- *Correlation coefficient (CC):* The correlation coefficient value is calculated for each pair of axes as follows:

$$CC = \frac{\sum_{i=1}^{N} (V_{cxi} - \bar{V}_{cx})(V_{cyi} - \bar{V}_{cy})}{\sqrt{\sum_{i=1}^{N} (V_{cxi} - \bar{V}_{cx})^2} \sqrt{\sum_{i=1}^{N} (V_{cyi} - \bar{V}_{cy})^2}}, \tag{33}$$

where V_{cxi} and V_{cyi} are the compensated velocities of each pair of axes in each dynamic phase of each stride, $\bar{V}_{cx}$ and $\bar{V}_{cy}$ are the mean values of V_{cxi} and V_{cyi}, and N is the number of measurements in each dynamic phase of each stride.

However, variation in the range of values of the aforementioned features may influence the classification results. Thus we utilize the Z-score method to normalize each feature for eliminating the effects of the variation. The normalization equation is shown as follows:

$$z = \frac{x - \mu}{\sigma}, \tag{34}$$

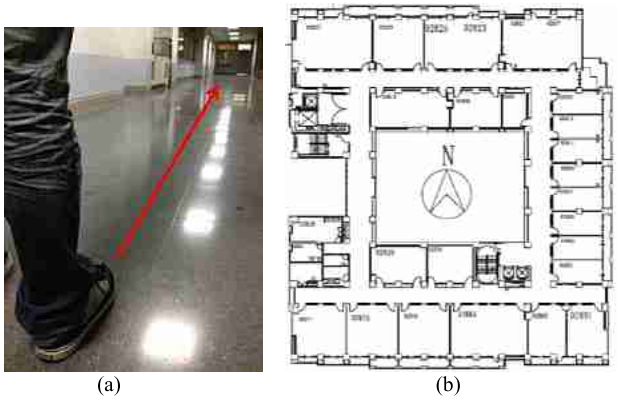

Fig. 11. The indoor experimental settings of the pedestrian trajectory reconstruction. (a) Actual indoor environment. (b) The eighth floor plane of the Electrical Engineering Building at National Cheng Kung University.

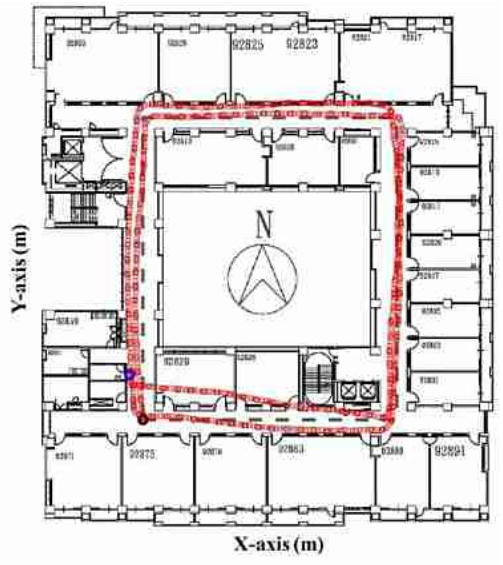

Fig. 12. Experimental results in the indoor environment. Gray color: Reference path. Red color: With the double-stage quaternion-based EKF orientation estimation. Black point: Start point. Blue point: End point.

where z is the normalized feature value, x is the original feature value, μ is the mean value of the original feature, and σ is the standard deviation value of the original feature.

2) Feature Reduction: Generally, redundant features increases the computational complexity and decreases the performance of classifiers. In this paper, the principal component analysis (PCA) and the linear discriminant analysis (LDA) are utilized to reduce the dimensions of the normalized features effectively and improve the classification performance [31]. The PCA is used to find the significant feature vectors in a projected space, while the LDA is employed to maximize the between-class distance and minimize the within-class distance. The two feature reduction methods are introduced in detail as follows.

a) Principal component analysis: The goal of the PCA is to transform the original feature vectors in a k-dimensional space ($\mathbf{x}_i \in \mathbb{R}^k$) into the reduced feature vectors in a p-dimensional space ($\mathbf{y}_i \in \mathbb{R}^p$) through a transformation

TABLE I

PARAMETERS USED IN THE DOUBLE-STAGE EXTENDED KALMAN FILTER

	$\mathbf{Q}$	$\mathbf{R}_a$	$\mathbf{R}_m$	$\widehat{\mathbf{P}}_t$
Parameters	$10^{-4}\times\begin{bmatrix}0.09937 & 0 & 0\\ 0 & 2.12685 & 0\\ 0 & 0 & 1.99226\end{bmatrix}$	$10^{-5}\times\begin{bmatrix}5.1621 & 0 & 0\\ 0 & 3.7677 & 0\\ 0 & 0 & 4.9745\end{bmatrix}$	$10^{-4}\times\begin{bmatrix}2.92112 & 0 & 0\\ 0 & 2.27993 & 0\\ 0 & 0 & 2.09759\end{bmatrix}$	$\begin{bmatrix}0.15 & 0.005 & 0.005 & 0.005\\ 0.005 & 0.15 & 0.005 & 0.005\\ 0.005 & 0.005 & 0.15 & 0.005\\ 0.005 & 0.005 & 0.005 & 0.15\end{bmatrix}$

TABLE II

ERROR COMPARISONS FOR THE INDOOR ENVIRONMENT EXPERIMENT

Algorithms	Quaternion-based EKF	[6]	[22]	[11]	[34]
Total Traveled Distance (m)	239.9	118.5	80	132	84.4
End-to-End Error (m)	4.81	--	0.3	4.31	--
End-to-End Positioning Accuracy (%)	2.01	0.3	0.4	3.26	3.38
Estimated Distance (m)	231.57	--	--	--	--
Distance Error (m)	8.33	--	--	--	--
Distance Error of Traveled Distance (%)	3.47	--	--	--	--

(a) (b)

Fig. 13. The outdoor experimental settings of the pedestrian trajectory reconstruction. (a) Actual outdoor environment. (b) Experimental results in the outdoor environment. Red color: With the double-stage quaternion-based EKF orientation estimation. Black point: Start point. Blue point: End point.

matrix ($\mathbf{W}$). At first, we calculate the mean ($\mathbf{m}$) of the original feature vectors and the covariance matrix ($\mathbf{S}$) in (35) and (36), respectively.

$$\mathbf{m} = \frac{1}{N}\sum_{i=1}^{N}\mathbf{x}_i, \tag{35}$$

$$\mathbf{S} = \frac{1}{N}\sum_{i=1}^{N}(\mathbf{x}_i - \mathbf{m})(\mathbf{x}_i - \mathbf{m})^T, \tag{36}$$

where N is the number of the strides. Through solving (37), the transformation matrix ($\mathbf{W}$) can be obtained by selecting the first p eigenvectors, which are sorted according to their corresponding eigenvalue (λ_i) in descending order:

$$\lambda_i\mathbf{e}_i = \mathbf{S}\mathbf{e}_i, \tag{37}$$

$$\mathbf{W} = \{\mathbf{e}_i\}_{i=1}^{p}, \tag{38}$$

where λ_i is the eigenvalue associated with the eigenvector $\mathbf{e}_i$. Finally, the original feature vectors ($\mathbf{x}_i \in \mathbb{R}^k$) can be transformed to reduced feature vectors ($\mathbf{y}_i \in \mathbb{R}^p$) through the transformation matrix ($\mathbf{W}$):

$$\mathbf{y}_i = \mathbf{W}^T\mathbf{x}_i. \tag{39}$$

b) Linear discriminant analysis: The goal of the LDA is to transform the original feature vectors ($\mathbf{x}_i \in \mathbb{R}^k$) into the reduced feature vectors ($\mathbf{y}_i \in \mathbb{R}^p$) by a transformation matrix ($\mathbf{W}$) which can maximize the ratio of the between-class scatter matrix ($\mathbf{S}_B$) to the within-class scatter matrix ($\mathbf{S}_w$). The within-class scatter matrix ($\mathbf{S}_w$) can be calculated as follows:

$$\mathbf{S}_w = \sum_{i=1}^{N}\sum_{j=1}^{n_i}(\mathbf{x}_j^{(i)} - \mathbf{m}_i)(\mathbf{x}_j^{(i)} - \mathbf{m}_i)^T, \tag{40}$$

where $\mathbf{x}_j^{(i)}$ is the j-th stride of the i-th class, $\mathbf{m}_i$ is the mean of the i-th class, n_i is the number of the strides in the i-th class, and N is the total number of the classes. Next, the between-class scatter matrix ($\mathbf{S}_B$) can be calculated as follows:

$$\mathbf{S}_B = \sum_{i=1}^{N} n_i(\mathbf{m}_i - \mathbf{m}_{all})(\mathbf{m}_i - \mathbf{m}_{all})^T, \tag{41}$$

where $\mathbf{m}_{all}$ represents the mean of all class. Note that $\mathbf{S}_w$ is the sum of the covariance matrices and $\mathbf{S}_B$ is the sum of the squared distances between the mean of each class and the mean of all classes. Subsequently, the transformation matrix ($\mathbf{W}$) can be obtained via maximizing the ratio of the between-class scatter matrix ($\mathbf{S}_B$) to the within-class scatter matrix ($\mathbf{S}_w$) as follows:

$$J(\mathbf{W}) = \frac{\mathbf{W}^T\mathbf{S}_B\mathbf{W}}{\mathbf{W}^T\mathbf{S}_w\mathbf{W}}, \tag{42}$$

where $\mathbf{W}^T\mathbf{S}_w\mathbf{W}$ and $\mathbf{W}^T\mathbf{S}_B\mathbf{W}$ are the new within-class scatter matrix and between-class scatter matrix in new feature space, respectively. Finally, the original feature vectors ($\mathbf{x}_i \in \mathbb{R}^k$) can be transformed to the reduced feature vectors ($\mathbf{y}_i \in \mathbb{R}^p$) through (39).

3) Probabilistic Neural Network Classifier: After the feature reduction step, we use the reduced gait features through the PCA, LDA, or PCA+LDA schemes as input features for a probabilistic neural network (PNN) classifier which classifies the walking patterns as level walking, walking upstairs, and walking downstairs. The PNN proposed by Specht is based on Baye's strategy for dealing with classification problems [32], and its outputs are the estimation of the probability of the class

TABLE III
ERROR COMPARISONS FOR THE OUTDOOR ENVIRONMENT EXPERIMENT

Algorithms	Quaternion-based EKF	[6]	[35]	[22]	[11]	[36]	[9]	[10]
Total Traveled Distance (m)	1020	741	1200	1100	332	437.5	60	2100
End-to-End Error (m)	2.66	2	10	5	3.88	3.58	--	--
End-to-End Positioning Accuracy (%)	0.26	0.3	0.8	0.45	1.17	0.82	--	--
Estimated Distance (m)	1014.72	--	--	--	--	438.69	58.8	--
Distance Error (m)	5.28	--	--	--	--	1.19	1.2	40
Distance Error of Traveled Distance (%)	0.52	--	--	--	--	0.27	2.0	1.9

(a) (b)

Fig. 14. The experiment settings of the trajectory height estimation experiment. (a) Walking upstairs. (b) Walking downstairs.

membership, where the training rule is based on the probability density functions of the classes. The structure of the PNN classifier shown in Fig. 7 is composed of an input layer, a pattern layer, a summation layer, and an output layer [33].

a) Input layer: The input features $\mathbf{x} = [x_1, x_2, \ldots, x_n]^T$ are conveyed to the neurons in the pattern layer directly, where n represents the number of the reduced features.

b) Pattern layer: The output of the neuron (P_{ki}) is derived by the multi-dimensional Gaussian function as follows:

$$P_{ki} = \frac{1}{(2\pi)^{n/2}\sigma^n} \exp\left[-\frac{(\mathbf{x}-\mathbf{x}_{ki})^T(\mathbf{x}-\mathbf{x}_{ki})}{2\sigma^2}\right], \quad (43)$$

where $\mathbf{x}_{ki}$ is the neuron vector, and σ is the smoothing parameter.

c) Summation layer: The neuron calculates the maximum likelihood of the input features $(\mathbf{x})$ belonging to the class k. The output of the neuron is calculated by averaging the outputs of all pattern layer neurons that belong to the same class:

$$S_k = \frac{1}{(2\pi)^{n/2}\sigma^n}\frac{1}{n_k}\sum_{i=1}^{n_k} exp\left[-\frac{(\mathbf{x}-\mathbf{x}_{ki})^T(\mathbf{x}-\mathbf{x}_{ki})}{2\sigma^2}\right], \quad (44)$$

where n_k is the total number of the strides in class k.

d) Output layer: The neuron compares the outputs of all neurons in the summation layer and decides the class numerical label as follows:

$$C = \text{argmax } S_k, \quad k = 1, 2, \ldots, N_c, \quad (45)$$

where C denotes the estimated class and N_c is the number of the classes. In this paper, the output of the PNN classifier is represented as the label of the three walking patterns (i.e., walking upstairs, level walking, and walking downstairs are labeled as '1', '2', and '3', respectively).

TABLE IV
CLASSIFICATION RATE OF THE PROPOSED FEATURE REDUCTION METHODS FOR THE TRAJECTORY HEIGHT ESTIMATION EXPERIMENT

Method	PCA+PNN	LDA+PNN	PCA+LDA+PNN
Classification Rate	95.9%	96.3%	97.0%
Dimensions	18	2	2 (18,2)

4) Height Estimation: Once the walking patterns are classified as walking upstairs, level walking, and walking downstairs through the PNN classifier, the estimation of the height for the indoor trajectory reconstruction can be obtained through the following equation.

$$L_z = \begin{cases} +h & \text{for walking upstairs} \\ 0 & \text{for level walking} \\ -h & \text{for walking downstairs,} \end{cases} \quad (46)$$

where L_z is the walking trajectory height and h is the height of each stair.

IV. EXPERIMENTAL RESULTS

In this section, the pedestrian trajectory reconstruction algorithm is validated via the experimental results of the sensor calibration, pedestrian trajectory reconstruction, and trajectory height estimation in indoor and outdoor environments. In the abovementioned experiments, we compared the trajectories reconstructed by the pedestrian trajectory reconstruction algorithm with some existing literatures. For the indoor and outdoor environments, all actual walks start and end at the same position. Hence, the end-to-end (starting point to ending point) error (e_p) and its positioning accuracy (e_{pa}) utilized for evaluating the accuracy of the reconstructed trajectories can be computed as follows.

$$e_p = \sqrt{(L_{cx} - \hat{L}_{cx})^2 + (L_{cy} - \hat{L}_{cy})^2}, \quad (47)$$

$$e_{pa} = \frac{\sqrt{(L_{cx} - \hat{L}_{cx})^2 + (L_{cy} - \hat{L}_{cy})^2}}{total\ traveled\ distance} \times 100\%, \quad (48)$$

where (L_{cx}, L_{cy}) is the ideal location of the reconstructed trajectory and $(\hat{L}_{cx}, \hat{L}_{cy})$ is the actual location of the ideal trajectory.

A. Sensor Calibration Experiment

In the accelerometer calibration experiment, we placed the accelerometer on a leveled surface and pointing each axis alternately upward and downward, and then kept it stationary

TABLE V
RESULTS OF WALKING PATTERN CLASSIFICATION

Actual \ Classified	Walking upstairs	Level walking	Walking downstairs	Classification rate (%)
Walking upstairs	219	5	1	97.3
Level walking	1	109	3	96.5
Walking downstairs	4	3	217	96.9

to observe the precision of the accelerations before and after calibrating the accelerometer. When the triaxial accelerometer was stationary, the measurement of the axis of the triaxial accelerometer, which was aligned with the Earth's gravity, should be equal to 1 g, and the measurements of the other axes of the accelerometer should be equal to zero. Figs. 8(a)-(c) show the experimental results of the accelerations before and after calibration process. Also, the SVM of the accelerations should be equal to 1 g when the accelerometer was placed randomly and stationary, and the experimental result is shown as Fig. 8(d). Obviously, the calibrated accelerations are more accurate than the uncalibrated accelerations.

In the gyroscope calibration experiment, we placed the gyroscope on a rotation stage and then rotated the triaxial gyroscope by the rotation stage which supplied a 360 °/s reference angular rate. When the triaxial gyroscope was rotated, the measurement of the axis of the triaxial gyroscope should be equal to 360 °/s, and the measurements of the other axes of the gyroscope should be equal to zero. Figs. 9(a)-(c) show the experimental results of the angular velocities before and after calibration process. In addition, the SVM of the angular velocities should also be equal to 360 °/s when the gyroscope was placed randomly and rotated by the rotation stage, and the experimental result is shown as Fig. 9(d). Similarly, the calibrated angular velocities are more accurate than the uncalibrated angular velocities.

For the calibration of the triaxial magnetometer, we rotated the magnetometer uniformly in a 3D space of the Earth's magnetic field without any magnetic disturbance. Theoretically, the magnetic signals in a 3D space should be a standard sphere and the coordinate of the center of the sphere is (0,0,0). Fig. 10(a) shows the magnetic signals before the calibration process in a 3D space, which was a ellipsoid and the coordinate of the center of the ellipsoid was (0.26,0.12,-0.12). After the magnetometer calibration process, the magnetic signals in a 3D space shown in Fig. 10(b) became a standard sphere and the coordinate of the center of the sphere was (-0.01,0.01,-0.02). Furthermore, we placed the magnetometer horizontally on the rotation stage and rotated at sequential rates of the following yaw angles ($+45° \rightarrow +90° \rightarrow +135° \rightarrow \pm 180° \rightarrow -135° \rightarrow -90° \rightarrow -45°$). Fig. 10(c) shows the yaw angles estimated by the calibrated and uncalibrated magnetic signals, respectively. Obviously, the yaw angles estimated by the calibrated magnetic signals are more accurate than that estimated by the uncalibrated magnetic signals. After the calibration procedure, the calibration matrices for the accelerometer, gyroscope, and magnetometer are $\mathbf{C}_a = \begin{bmatrix} 1.0184 & 0 & 0 & -0.0104 \\ 0 & 1.0047 & 0 & 0.0108 \\ 0 & 0 & 1.0022 & -0.0457 \end{bmatrix}$, $\mathbf{C}_g = \begin{bmatrix} 1.0989 & 0 & 0 & -0.0234 \\ 0 & 1.0979 & 0 & 0.0004 \\ 0 & 0 & 1.0928 & 0.0013 \end{bmatrix}$, and $\mathbf{C}_m = \begin{bmatrix} 8.2655 & 0 & 0 & 0.2453 \\ 0 & 8.5072 & 0 & 0.1689 \\ 0 & 0 & 8.1313 & 0.0738 \end{bmatrix}$, respectively.

B. Indoor Pedestrian Location Experiment

The indoor environment experiment was performed on the eighth floor of the Electrical Engineering Building at National Cheng Kung University. The total distance of the rectangular passage is about 119.95 meters. Subjects were asked to walk twice along a square-shaped line on the eighth floor at normal speed without any external localization techniques. The total traveled distance of the indoor environment experiment is about 239.9 meters and the end point of the walking path is at the same location as the start point. Fig. 11 shows the actual indoor environment and its floor plan layout. Fig. 12 shows the reconstructed trajectory in the indoor environment from one participant in particular, which was reconstructed by the pedestrian trajectory reconstruction algorithm with the quaternion-based EKF orientation estimation method. The end-to-end (starting point to ending point) error (e_p) of the reconstructed trajectory using the pedestrian trajectory reconstruction algorithm with the EKF was 4.81 m. Hence, the end-to-end positioning accuracy (e_{pa}) was around 2.01% of the total traveled distance for the double-stage quaternion-based EKF algorithm. In Fig. 12, the distance error was 8.33 m (3.47% of total traveled distance) using the double-stage quaternion-based EKF algorithm. Table I shows the values of the white noise covariance matrix of the filtered angular velocity ($\mathbf{Q}$), white noise covariance matrix of the filtered acceleration ($\mathbf{R}_a$), white noise covariance matrix of the magnetic north vector ($\mathbf{R}_m$), and the initial value of the state error covariance matrix $\hat{\mathbf{P}}_t$. Table II shows the performance comparison of the proposed pedestrian trajectory reconstruction algorithm and 4 existing methods for the indoor pedestrian location experiment. The result compares with the result reported in [6], [22], [11], and [34] whose average indoor end-to-end positioning accuracy are 0.3%, 0.4%, 3.26%, and 3.38% of the gold standard distance. Hence, the experimental results show that the proposed pedestrian trajectory reconstruction algorithm with the quaternion-based EKF orientation estimation method is effective to provide accurate reconstructed trajectory in an indoor environment.

C. Outdoor Pedestrian Location Experiment

The outdoor environment experiment was performed on the Tzu-Chiang campus in National Cheng Kung University. The total distance of the road is approximately 510 meters. Subjects were asked to walk twice along a square-shaped line on the road at normal speed without any external localization techniques. The total traveled distance of the outdoor environment experiment is approximately 1020 meters and the end point of the walking path is at the same location as the

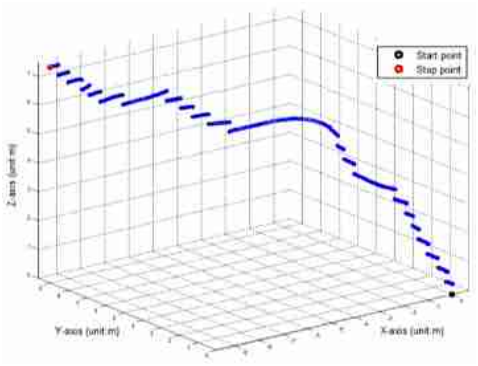

Fig. 15. The reconstructed trajectory for walking upstairs.

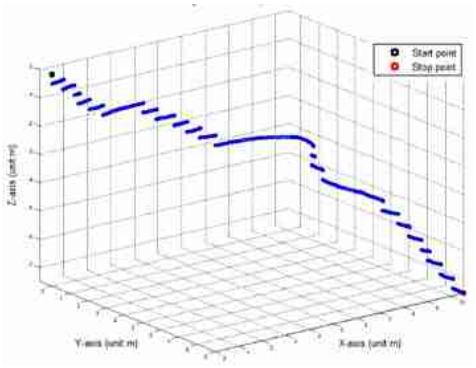

Fig. 16. The reconstructed trajectory for walking downstairs.

start point. Fig. 13(a) shows the outdoor environment. The overall accuracy of the pedestrian trajectory reconstruction algorithm with the quaternion-based EKF method was evaluated by comparing with a reference trajectory on Google map. Fig. 13(b) shows the reconstructed trajectory in the outdoor environment, which was reconstructed by the pedestrian trajectory reconstruction algorithm with the quaternion-based EKF method. Similarly, the trajectory reconstructed by the pedestrian trajectory reconstruction algorithm with the quaternion-based EKF is close to the ideal close square loop. Table III shows the performance comparison of the proposed pedestrian trajectory reconstruction algorithm and 7 existing methods for the outdoor pedestrian location experiment. The end-to-end (starting point to ending point) error (e_p) of the reconstructed trajectory using the pedestrian trajectory reconstruction algorithm with the quaternion-based EKF was 2.66 m for a trajectory of 1020 m (0.26% of the total traveled distance). In Fig. 13(b), the overall error in distance was about 5.28 m (0.52% of total traveled distance) using the double-stage quaternion-based EKF algorithm. The outdoor positioning accuracy compares favorably with those presented in the literature. The end-to-end positioning accuracy are 0.3%, 0.8%, 0.45%, 1.17%, and 0.82% of the traveled distance reported in [6], [35], [22], [11], and [36], respectively. The distance errors of the overall traveled distance presented in [36], [9], and [10] are 0.27%, 2%, and 1.9%, respectively. Hence, the experimental results show that the proposed pedestrian trajectory reconstruction algorithm with the quaternion-based EKF orientation estimation method can estimate traveled distance accurately in an outdoor environment.

D. Trajectory Height Estimation Experiment

In the trajectory height estimation experiment, the participant wore the wearable inertial pedestrian navigation system on the foot and walked upstairs, downstairs, and levelly from the first floor to third floor in the Electrical Engineering Building at National Cheng Kung University. The trajectory path of the walking upstairs can be described as: upstairs → level walking → upstairs → level walking → upstairs → level walking → upstairs. Similarly, the trajectory path of the walking downstairs can be described as: downstairs → level walking → downstairs → level walking → downstairs → level walking → downstairs. The total height of the stairs is 7.48 meters wherein the height of each stair is about 17 cm. Fig. 14 shows the experimental environment for the trajectory height estimation. A total of 225, 113, 224 strides were recorded in this experiment for the walking upstairs, level walking, and walking downstairs conditions, respectively. With the compensated walking velocities, 21 gait features were generated by the feature extraction procedure. After the normalization, the normalized features were chosen as characteristic features through the PCA, LDA, or PCA+LDA schemes. Finally, the reduced gait features were used as input features for the probabilistic neural network (PNN) classifier to classify the walking patterns as level walking, walking upstairs, and walking downstairs. From Table IV, the feature reduced method (PCA+LDA) with the PNN classifier obtained the best classification performance. The dimension of the gait features in each dynamic phase within each stride was first reduced from 21 to 18 using the PCA method. Subsequently, the PCA-based features were treated as the inputs for the LDA whose dimension were reduced from 18 to 2. The confusion matrix for the classification scheme by using the PCA+LDA+PNN scheme is shown in Table V. The best classification accuracy was obtained for walking upstairs (97.3%) while the worst classification accuracy is obtained for level walking (96.5%). The overall classification rate is about 97.0%. Thus, the walking strides can be classified by the trajectory height estimation algorithm effectively. The average height errors for the walking upstairs and walking downstairs were 3.60% and 6.42%, respectively. Figs. 15 and 16 show the reconstructed trajectories for the walking upstairs and downstairs from one participant in particular, demonstrating that the walking trajectories can be reconstructed by the pedestrian trajectory reconstruction algorithm accurately.

V. Conclusions

In this paper, a wearable inertial pedestrian navigation system and its associated pedestrian trajectory reconstruction algorithm have been developed to reduce the intrinsic errors and drifts of the inertial sensors for obtaining more accurate pedestrian walking trajectories. The pedestrian trajectory reconstruction algorithm is composed of inertial signal acquisition, signal preprocessing, trajectory reconstruction, and trajectory height estimation. The proposed algorithm can reconstruct pedestrian walking trajectories in indoor and

outdoor environments. The end-to-end (starting point to ending point) error and the distance error in the indoor environment were around 4.81 m (2.01% of total traveled distance) and 8.33 m (3.47% of total traveled distance). The end-to-end (starting point to ending point) error and the distance error in the outdoor environment were around 2.66 m (0.26% of total traveled distance) and 5.28 m (0.52% of total traveled distance). The overall classification rate for walking patterns (walking upstairs, level walking, and walking downstairs) was 97.0%. The average height errors of the walking upstairs and walking downstairs were 3.60% and 6.42%, respectively. Based on the above experimental results, we believe that the wearable inertial pedestrian navigation system and its associated pedestrian trajectory reconstruction algorithm will be provide a novel and effective contribution to pedestrian navigation system design.

REFERENCES

[1] J. Hightower and G. Borriello, "Location systems for ubiquitous computing," *Computer*, vol. 34, no. 8, pp. 57–66, 2001.

[2] H. Liu, H. Darabi, P. Banerjee, and J. Liu, "Survey of wireless indoor positioning techniques and systems," *IEEE Trans. Syst., Man, Cybern. C, Appl. Rev.*, vol. 37, no. 6, pp. 1067–1080, Nov. 2007.

[3] R. Tesoriero, J. Gallud, M. Lozano, and V. Penichet, "Using active and passive RFID technology to support indoor location-aware systems," *IEEE Trans. Consum. Electron.*, vol. 54, no. 2, pp. 578–583, May 2008.

[4] S. H. Fang and T. N. Lin, "Indoor location system based on discriminant-adaptive neural network in IEEE 802.11 environments," *IEEE Trans. Neural Netw.*, vol. 19, no. 11, pp. 1973–1978, Nov. 2008.

[5] A. Correa, M. Barcelo, A. Morell, and J. Lopez Vicario, "Enhanced inertial-aided indoor tracking system for wireless sensor networks: A review," *IEEE Sensors J.*, vol. 14, no. 9, pp. 2921–2929, Sep. 2014.

[6] E. Foxlin, "Pedestrian tracking with shoe-mounted inertial sensors," *IEEE Comput. Graph. Appl.*, vol. 25, no. 6, pp. 38–46, Nov./Dec. 2005.

[7] W. Kang and Y. Han, "SmartPDR: Smartphone-based pedestrian dead reckoning for indoor localization," *IEEE Sensors J.*, vol. 15, no. 5, pp. 2906–2916, May 2015.

[8] Y. Zhuang and N. El-Sheimy, "Tightly-coupled integration of WiFi and MEMS sensors on handheld devices for indoor pedestrian navigation," *IEEE Sensors J.*, vol. 16, no. 1, pp. 224–234, Jan. 2016.

[9] C. Huang, Z. Liao, and L. Zhao, "Synergism of INS and PDR in self-contained pedestrian tracking with a miniature sensor module," *IEEE Sensors J.*, vol. 10, no. 8, pp. 1349–1359, Aug. 2010.

[10] H. Zhang, W. Yuan, Q. Shen, T. Li, and H. Chang, "A handheld inertial pedestrian navigation system with accurate step modes and device poses recognition," *IEEE Sensors J.*, vol. 15, no. 3, pp. 1421–1429, Mar. 2015.

[11] X. Meng, Z.-Q. Zhang, J.-K. Wu, W.-C. Wong, and H. Yu, "Self-contained pedestrian tracking during normal walking using an inertial/magnetic sensor module," *IEEE Trans. Biomed. Eng.*, vol. 61, no. 3, pp. 892–899, Mar. 2014.

[12] A. M. Sabatini, "Quaternion-based extended Kalman filter for determining orientation by inertial and magnetic sensing," *IEEE Trans. Biomed. Eng.*, vol. 53, no. 7, pp. 1346–1356, Jul. 2006.

[13] Y. S. Suh, "Orientation estimation using a quaternion-based indirect Kalman filter with adaptive estimation of external acceleration," *IEEE Trans. Instrum. Meas.*, vol. 59, no. 12, pp. 3296–3305, Dec. 2010.

[14] L. Wang, Z. Zhang, and P. Sun, "Quaternion-based Kalman filter for AHRS using an adaptive-step gradient descent algorithm," *Int. J. Adv. Robot. Syst.*, vol. 12, p. 131, Sep. 2015.

[15] S. Sabatelli, M. Galgani, L. Fanucci, and A. Rocchi, "A double-stage Kalman filter for orientation tracking with an integrated processor in 9-D IMU," *IEEE Trans. Instrum. Meas.*, vol. 62, no. 3, pp. 590–598, Mar. 2013.

[16] J. L. Crassidis and F. L. Markley, "Attitude estimation using modified rodrigues parameters," in *Proc. Flight Mech./Estimation Theory Symp.*, 1996, pp. 71–83.

[17] L.-H. Chen, E. H.-K. Wu, M.-H. Jin, and G.-H. Chen, "Intelligent fusion of Wi-Fi and inertial sensor-based positioning systems for indoor pedestrian navigation," *IEEE Sensors J.*, vol. 14, no. 11, pp. 4034–4042, Nov. 2014.

[18] H. Hyyti and A. Visala, "A DCM based attitude estimation algorithm for low-cost MEMS IMUs," *Int. J. Navigat. Observat.*, vol. 2015, Nov. 2015, Art. no. 503814.

[19] X. Yuan, S. Yu, S. Zhang, G. Wang, and S. Liu, "Quaternion-based unscented Kalman filter for accurate indoor heading estimation using wearable multi-sensor system," *Sensors*, vol. 15, no. 5, pp. 10872–10890, 2015.

[20] J. L. Crassidis and F. L. Markley, "Unscented filtering for spacecraft attitude estimation," *J. Guid., Control, Dyn.*, vol. 26, no. 4, pp. 536–542, Jul. 2003.

[21] A. Masiero, A. Guarnieri, F. Pirotti, and A. Vettore, "A particle filter for smartphone-based indoor pedestrian navigation," *Micromachines*, vol. 5, no. 4, pp. 1012–1033, 2014.

[22] H. Fourati, "Heterogeneous data fusion algorithm for pedestrian navigation via foot-mounted inertial measurement unit and complementary filter," *IEEE Trans. Instrum. Meas.*, vol. 64, no. 1, pp. 221–229, Jan. 2015.

[23] W.-C. Bang, W. Chang, K.-H. Kang, E.-S. Choi, A. Potanin, and D.-Y. Kim, "Self-contained spatial input device for wearable computers," in *Proc. 7th Int. Symp. Wearable Comput.*, Oct. 2005, pp. 26–34.

[24] Y.-L. Hsu, C.-L. Chu, Y.-J. Tsai, and J.-S. Wang, "An inertial pen with dynamic time warping recognizer for handwriting and gesture recognition," *IEEE Sensors J.*, vol. 15, no. 1, pp. 154–163, Jan. 2015.

[25] Z. F. Syed, P. Aggarwal, C. Goodall, X. Niu, and N. El-Sheimy, "A new multi-position calibration method for MEMS inertial navigation systems," *Meas. Sci. Technol.*, vol. 18, no. 7, pp. 1897–1907, 2007.

[26] D. Roetenberg, H. J. Luinge, C. T. M. Baten, and P. H. Veltink, "Compensation of magnetic disturbances improves inertial and magnetic sensing of human body segment orientation," *IEEE Trans. Neural Syst. Rehabil. Eng.*, vol. 13, no. 3, pp. 395–405, Sep. 2005.

[27] C. C. Foster and G. H. Elkaim, "Extension of a two-step calibration methodology to include nonorthogonal sensor axes," *IEEE Trans. Aerosp. Electron. Syst.*, vol. 44, no. 3, pp. 1070–1078, Jul. 2008.

[28] J. B. Kuipers, *Quaternions and Rotation Sequences*. Princeton, NJ, USA: Princeton Univ. Press, 1999.

[29] Y.-L. Hsu *et al.*, "Gait and balance analysis for patients with Alzheimer's disease using an inertial-sensor-based wearable instrument," *IEEE J. Biomed. Health Inform.*, vol. 18, no. 6, pp. 1822–1830, Nov. 2014.

[30] S.-W. Lee and K. Mase, "Activity and location recognition using wearable sensors," *IEEE Pervasive Comput.*, vol. 1, no. 3, pp. 24–32, Jul./Sep. 2002.

[31] M. Karg, K. Kuhnlenz, and M. Buss, "Recognition of affect based on gait patterns," *IEEE Trans. Syst. Man, Cybern. B, Cybern.*, vol. 40, no. 4, pp. 1050–1061, Aug. 2010.

[32] D. F. Specht, "Probabilistic neural networks," *Neural Netw.*, vol. 3, no. 1, pp. 109–118, 1990.

[33] Y. Wang, L. Li, J. Ni, and S. Huang, "Feature selection using tabu search with long-term memories and probabilistic neural networks," *Pattern Recognit. Lett.*, vol. 30, no. 7, pp. 661–670, 2009.

[34] J. Torres-Solis and T. Chau, "Wearable indoor pedestrian dead reckoning system," *Pervasive Mobile Comput.*, vol. 6, no. 3, pp. 351–361, 2010.

[35] L. Fang *et al.*, "Design of a wireless assisted pedestrian dead reckoning system-the NavMote experience," *IEEE Trans. Instrum. Meas.*, vol. 54, no. 6, pp. 2342–2358, Dec. 2005.

[36] X. Yun, J. Calusdian, E. R. Bachmann, and R. B. McGhee, "Estimation of human foot motion during normal walking using inertial and magnetic sensor measurements," *IEEE Trans. Instrum. Meas.*, vol. 61, no. 7, pp. 2059–2072, Jul. 2012.

Yu-Liang Hsu (M'17) received the B.S. degree in automatic control engineering from Feng Chia University, Taichung, Taiwan, in 2004, and the M.S. and Ph.D. degrees in electrical engineering from National Cheng Kung University, Tainan, Taiwan, in 2007 and 2011, respectively.

He is currently an Assistant Professor with the Department of Automatic Control Engineering, Feng Chia University. His research interests include computational intelligence, nonlinear system identification, biomedical signal processing, and inertial sensing applications.

Jeen-Shing Wang (S'94–M'02) received the B.S. and M.S. degrees in electrical engineering from the University of Missouri, Columbia, USA, in 1996 and 1997, respectively, and the Ph.D. degree from Purdue University, West Lafayette, IN, USA, in 2001.

He is currently a Distinguished Professor with the Department of Electrical Engineering, National Cheng Kung University, Taiwan. His research interests include computational intelligence, design of wearables, big data analysis, and system optimization.

Che-Wei Chang received the B.S. degree in electrical and computer engineering from National Chiao Tung University in 2011 and the M.S. degree in electrical engineering from National Cheng Kung University, Taiwan, in 2013.

His research interests include signal processing and inertial sensing.